small NANO MICRO

Interfaces

Direct Measurements of the Mechanical Strength of Carbon Nanotube–Poly(methyl methacrylate) Interfaces

*Xiaoming Chen, Meng Zheng, Cheol Park, and Changhong Ke**

***U**nderstanding the interfacial stress transfer between carbon nanotubes (CNTs) and polymer matrices is of great importance to the development of CNT-reinforced polymer nanocomposites. In this paper, an experimental study is presented of the interfacial strength between individual double-walled CNTs and poly(methyl methacrylate) (PMMA) using an in situ nanomechanical single-tube pull-out testing scheme inside a high-resolution electron microscope. By pulling out individual tubes with different embedded lengths, this work reveals the shear lag effect on the nanotube–polymer interface and demonstrates that the effective interfacial load transfer occurs only within a certain embedded length. These results show that the CNT–PMMA interface possesses an interfacial fracture energy within 0.054–0.80 J/m^2 and a maximum interfacial strength within 85–372 MPa. This work is useful to better understand the local stress transfer on nanotube–polymer interfaces.*

1. Introduction

The unique light-weight and high-strength characteristics of fiber-reinforced polymer nanocomposites are attractive for a number of structural applications ranging from bodies of aerospace shuttles and aircraft to automobile components.[1] Carbon nanotubes (CNTs), a light and strong one-dimensional tubular nanostructure, hold great promise as reinforcing additives for polymer nanocomposites.[2] However, the mechanical performance of CNT-reinforced polymers is still far from reaching the anticipated level even though significant advances have been achieved so far.[3] Understanding the interfacial stress transfer and ultimately having a good command of the nanotube–polymer interface (e.g. via surface functionalization) are one of the key scientific challenges to be tackled.[4] To date, a vast majority of the studies on CNT-reinforced polymers were performed at macroscopic level and yielded merely bulk material properties. The interfacial strength properties can only be evaluated qualitatively and indirectly from macroscopic measurements. Reports on direct and quantitative measurements of the interfacial strength between individual CNTs and polymers based on microscopic-level single-tube pull-out testing techniques remain quite limited.[5–12] The seemingly simple testing scheme of pulling out individual tubes from surrounding matrices actually poses many technical difficulties. For instance, the embedded portion of the tube needs to stay in a planar and straight manner and the pulling force must be well aligned with the tube axis to avoid any bending effect. It is extremely challenging to grab the free end of the tube and to apply and quantify the pulling load, while monitoring the mechanical response of the tested tube at adequate force and spatial resolutions. In addition, even though single- or few-walled CNTs have been widely used as reinforcing nano-fillers in polymers,[13–16] direct measurements of the interfacial stress transfer between polymers and CNTs of sub-10 nm in outer diameter remain largely unexplored. In this paper, we report a single-tube pull-out testing

X.-M. Chen, M. Zheng, Prof. C.-H. Ke
Department of Mechanical Engineering
State University of New York at Binghamton
Binghamton, NY, 13902, USA
E-mail: cke@binghamton.edu
Dr. C. Park
National Institute of Aerospace
Hampton, VA 23666, USA
Dr. C. Park
Department of Mechanical and Aerospace Engineering
University of Virginia
Charlottesville, VA 22904, USA

DOI: 10.1002/smll.201202771

scheme based on in situ nanomechanical characterization techniques inside a scanning electron microscopy (SEM) and quantitatively characterize the interfacial strength between individual double-walled CNTs (DWCNTs) and poly(methyl methacrylate) (PMMA). By pulling out individual tubes with different embedded lengths, our work reveals the shear lag effect on the nanotube–polymer interface and demonstrates that the effective interfacial load transfer occurs only within a certain embedded length.

2. Results and Discussion

Figure 1a illustrates our in situ nanomechanical single-tube pull-out testing scheme inside an SEM. Figure 1b shows the cross-section schematic of the testing scheme, in which a nanotube with an outer diameter D_{nt} and an initial embedded length l is being pulled out of a thin-film polymer with a total thickness t by a stretching force P. The nanotube–polymer interface is formed inside a polymer/nanotube/polymer sandwich structure, in which a free-standing cantilevered nanotube is partially embedded into a thin-film polymer. One pre-calibrated AFM cantilever, which is mounted on a 3D piezo stage, is used to first grip the free end of the protruding nanotube and then displaced to apply a tensile force to pull the tube out of the polymer. Only those tubes, whose axes are perpendicular to the AFM cantilever orientation and thus aligned with the pulling force direction, are chosen for the pull-out test. With the aid of a high resolution electron beam, the mechanical deformation/displacement of both the nanotube and the AFM cantilever can be visualized in situ with resolutions of a few nanometers during the pull-out process. It is envisioned that this testing scheme enables the pull-out measurement to be performed in a quantitative and well-controlled manner and can be used to test interfaces formed by a wide variety of polymers (e.g. both thermoplastic and thermoset) and nanostructures with a broad range of diameters (i.e. from a few to hundreds of nanometers).

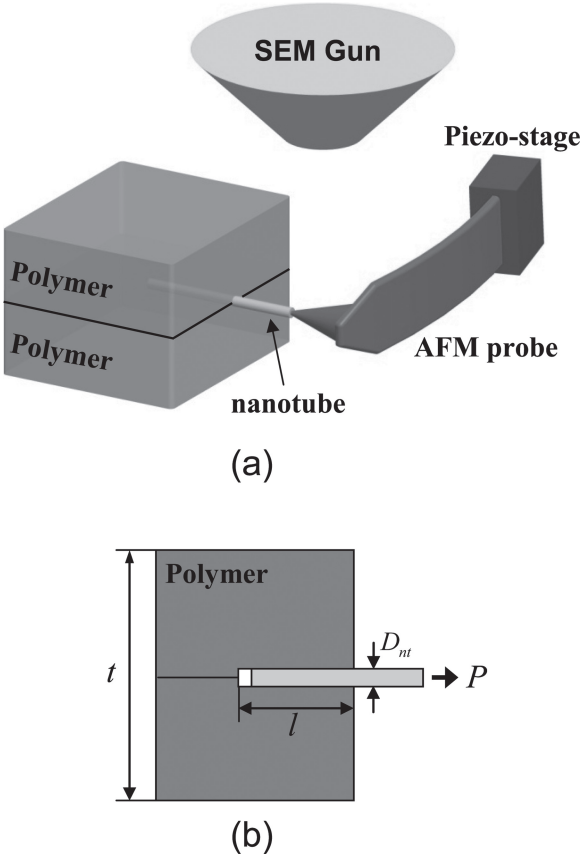

Figure 1. (a) 3D illustration of our in situ nanomechanical single-tube pull-out measurement inside a scanning electron microscope. (b) Cross-sectional schematic of the single-tube pull-out scheme shown in (a). P is the pull-out load, l is the tube embedded length, D_{nt} is the tube outer diameter, and t is the total thickness of the thin-film polymer.

DWCNTs with a nominal length of 50 μm were employed in this study. To ensure that individual tubes remain straight inside thin-film polymers, their tube lengths were shortened to be within 2 μm by means of adjusting the ultrasonication time during the nanotube dispersion process (see Experimental Section for details). **Figure 2**a shows a representative AFM image of dispersed nanotubes and their double-walled tubular structures were inspected and confirmed using transmission electron microscopy (TEM), as exemplified by the inset image. Figure 2b shows the diameter distribution of 400 dispersed nanotubes characterized by AFM, revealing that the tubes have a poly-dispersed outer diameter with an average value of 3.1 nm and are mostly within 2.0–4.2 nm (>92%). The surface chemistry of the dispersed nanotubes was also characterized by Fourier transform infrared spectroscopy (FTIR). Figure 2c shows a measured FTIR spectrum, which displays only two peaks centered around 1187 and 1578 cm^{-1}, respectively. The broadband located around 1187 cm^{-1} is assigned to *D*-band, while the peak at 1578 cm^{-1} is ascribed to the vibration of carbon skeleton of CNTs.[17,18] There are no discernable peaks in the stretching mode ranges of C=O (between 1600–1800 cm^{-1}), CH (between 2800–3000 cm^{-1}) and OH (between 3000–3600 cm^{-1}) groups, indicating the absence of these functional groups on the nanotubes' surfaces.

The CNT–PMMA samples employed in our in situ single-tube pull-out tests are three-layer sandwich structures, whose manufacturing processes are illustrated in **Figure 3**. In brief, a layer of well-dispersed CNTs is deposited on top of one thin-film PMMA layer by spin-coating, and subsequently covered by another PMMA layer (Figures 3a,b). After drying and by means of cracking and breaking the silicon substrate using a diamond scriber along its crystal orientation, the thin-film polymer breaks and some of the embedded tubes are exposed as free-standing cantilever structures (Figure 3c). Figure 3d shows one of our CNT–PMMA samples with protruding straight nanotubes prepared using this method. Our TEM inspection of protruding CNT samples, as exemplified by the image shown in Figure 3e, confirms their single-tube structures. Their tube diameters measured by TEM are consistent with our AFM imaging results. It is noted that, in this sample preparation method, the tubes remain straight and stay largely in the same plane and parallel to the surface of the thin-film polymer.

small NANO MICRO

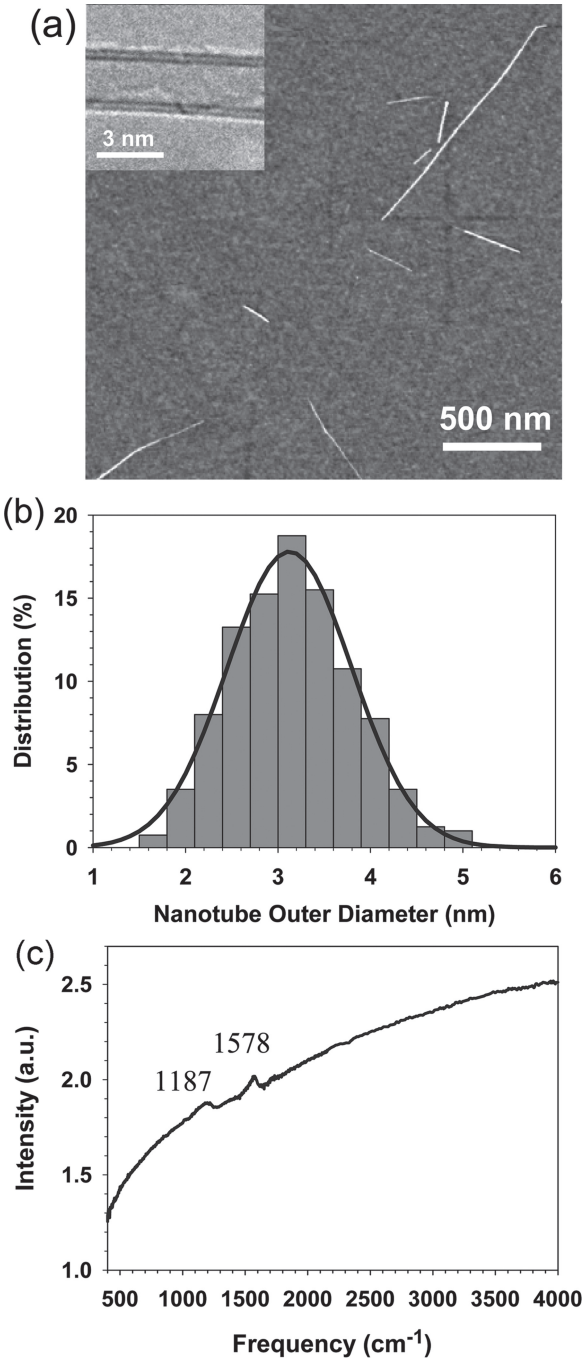

Figure 2. (a) One representative tapping mode AFM image of dispersed carbon nanotubes. The inset TEM image shows a double-walled tube of 2.9 nm in outer diameter. (b) The diameter distribution of the dispersed tubes measured by AFM (n = 400). (c) FTIR spectrum of the dispersed nanotubes.

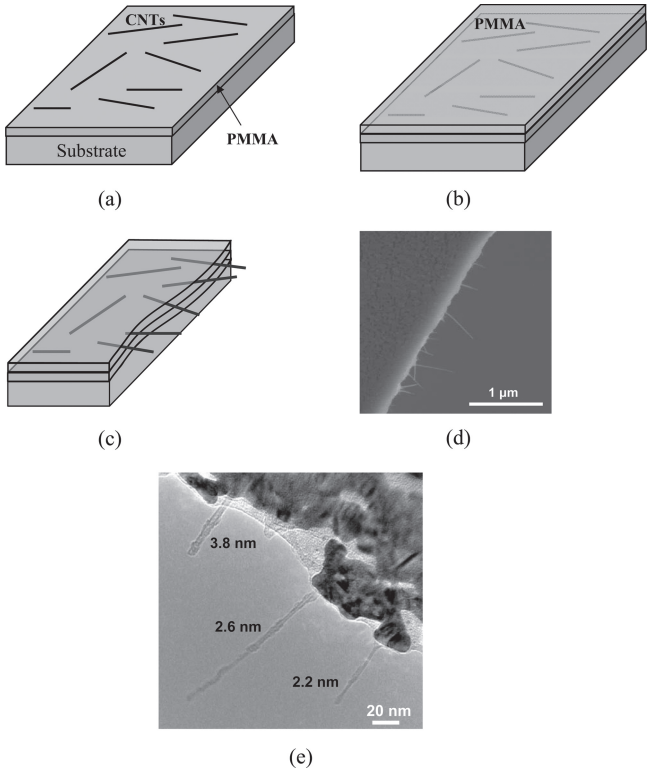

Figure 3. Schematic diagrams of the manufacturing processes of sandwich-like CNT–PMMA thin-film composites: (a) deposition of the first PMMA layer on the substrate, followed by the deposition of the CNT layer; (b) deposition of the second PMMA layer covering the nanotubes; (c) exposing the embedded CNTs by cracking and breaking the substrate; (d) SEM image of one representative CNT–PMMA sample employed in our single-tube pull-out tests; (e) TEM image of three protruding nanotubes from a PMMA matrix. The marked numbers are the measured tube outer diameters.

Figure 4a shows one of the AFM force sensors used in our single-tube pull-out tests. The AFM force sensor was placed vertically and its tip axis was perpendicular to the electron beam. Two scenarios for the outcome of our pull-out tests were experimentally observed: (1) the embedded tube segment was pulled out from the matrix; (2) the tube was fractured and its embedded portion remained inside the matrix. Most of our in situ pull-out measurements (20 out of 23 tests) fall into the first scenario. Figures 4b–d show three selected SEM snapshots of one representative single-tube pull-out test. Electron beam-induced deposition (EBID) of platinum (Pt)[19] was employed to ensure a firm attachment of the nanotube to the AFM tip. Our SEM observation shows that the pull-out of the nanotube occurred as a catastrophic failure of the CNT-polymer interface.[9] For this measurement, the pull-out force (P) and the embedded tube length (l) are measured to be 180 nN and 1.12 μm respectively. To the best of our knowledge, our work is the first reported single-tube pull-out measurements on CNT–PMMA interfaces. It is noted that the deposited Pt using EBID techniques inevitably covered the protruding portion of the tube through diffusion, resulting in a noticeable increase of its lateral thickness. The deposited Pt layer is anticipated to have no direct effect on the CNT–PMMA interface, thus its interfacial strength. The presence of the Pt layer helps determine the starting position of the embedded tube segment, thus the embedded tube length. The fracturing of the nanotube during the pull-out test was also observed and one representative measurement is shown in **Figure 5**. In this measurement, the tube was fractured at its protruding segment and its embedded portion

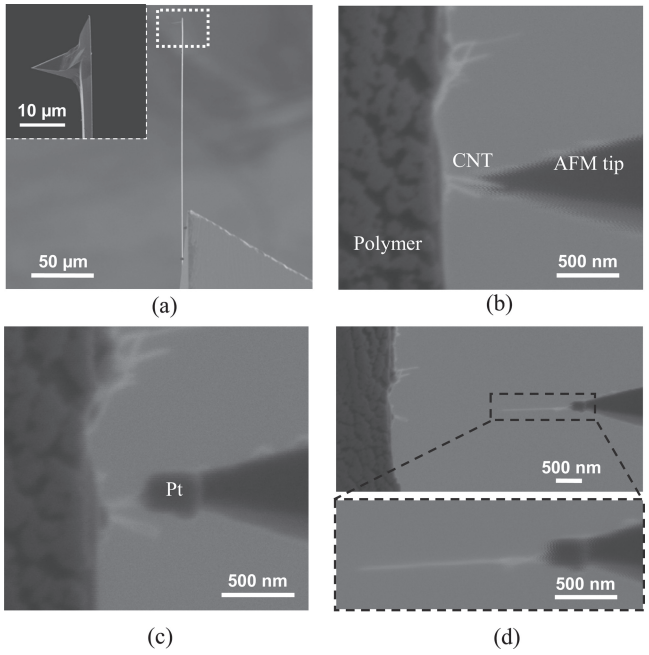

Figure 4. (a) SEM image of one of the AFM force sensors employed in our single-tube pull-out measurements; (b)–(d) selected SEM snapshots of pulling one tube out of the polymer: (b) the tip of an AFM force sensor was controlled to make contact with the free-end of a protruding nanotube; (c) the nanotube end was welded to the AFM tip using EBID of Pt; (d) the tube was pulled out from the polymer. The bottom image is a zoom-in view of the pulled-out tube.

inside the polymer remained intact. It is noted that the chance of the tube fracture at its embedded portion is quite low, if not impossible, because the normal stress in the tube is always higher at its protruding portion than its embedded segment. Because DWCNTs were used in our tests, it is possible that the outer tube shell, which is attached to the AFM force sensor, may be broken first, leading to a telescopic pull-out of the inner tube shell. It is noted that the lateral size of a DWCNT appears noticeably larger than that of its inner tube in the recorded SEM images, which was experimentally confirmed (see Figure S1 in the Supporting Information). Therefore, the telescopic pull-out scenario can be identified through a comparison of the lateral sizes of the protruding and the

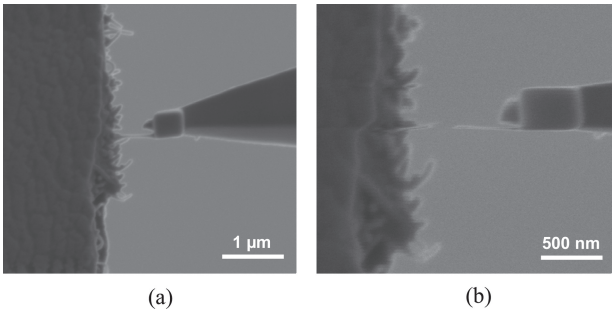

Figure 5. One representative measurement showing the fracture of a protruding tube segment during the pull-out test: (a) before and (b) after the tube fracture.

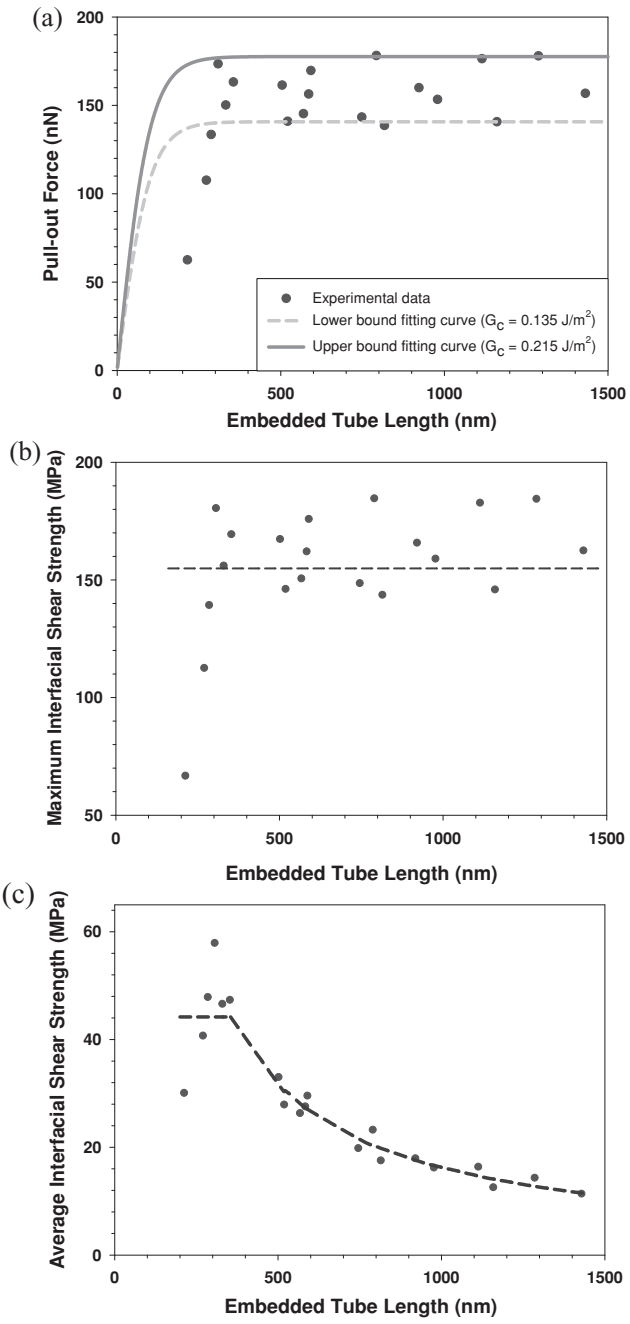

Figure 6. (a) The pull-out force versus the nanotube embedded length measured in our single-tube pull-out tests (dots) and the respective theoretical fitting curves along the lower and upper bounds of the measured pull-out force based on Equation (1) (solid and dotted curves). (b) The calculated maximum interfacial shear strength. The dotted line indicates the mean value of the whole data set. (c) The calculated average interfacial shear strength. The initial straight dotted line segment represents the mean value of the data set with the embedded tube length less than the critical value, while the decreasing segment represents a power fitting of the rest data set. All the calculated data points and theoretical curves are based on the median tube diameter.

pulled-out tube segments shown in the recorded SEM images. It is noted that none of our single-tube pull-out tests falls into this telescopic pull-out scenario. In our pull-out measurements, the nanotube–polymer interface was buried below a

NANO MICRO small

polymer film of ~0.8 μm in thickness and not exposed directly to the electron beam. Therefore, even though the electron beam irradiation may have a material effect on the strength of protruding nanotubes,[20] it is expected to have little-to-no effect on the nanotube–polymer interfacial strength.

Figure 6a shows the pull-out forces measured in 20 different single-tube pull-out tests with the embedded tube length ranging from 0.21 to 1.43 μm. Our results show that the pull-out force first increases with the embedded length (up to 310 nm), and then fluctuates within a narrow band range of 140–180 nN even after a several-fold increase of the embedded length. The observed fluctuation of the pull-out force is attributed to the variations of the nanotube–polymer interface and the nanotube diameter. The dependence of our measured pull-out force on the embedded tube length, as shown in Figure 6a, is consistent with the prediction of the fiber-polymer interfacial failure based on energy balance principle, which considers the nanotube pull-out process as interfacial debonding through crack propagation.[21] During the nanotube pull-out process, the released strain energy stored in the stretched tube supplies the energy required to propagate an interfacial crack through the bonded interface region. The interface debonding process leads to an unchanged pull-out load when the embedded length exceeds a threshold value named as "critical embedded length". This energy-driven pull-out process indicates that an effective interfacial shear load transfer between the nanotube and the polymer occurs only within the critical embedded length range and any further increase of the embedded length does not increase the shear load on the nanotube–polymer interface (if the friction force is not considered). This so-called "shear lag effect" on the nanotube–polymer interface[5,9] was clearly exhibited in our single-tube pull-out measurements, indicating that our experimental work is useful to better understand the local load transfer mechanism on the nanotube–polymer interface. Next we look at the quantification of the CNT–PMMA interfacial strength, focusing on two relevant physical quantities: interfacial fracture energy and interfacial shear strength.

Considering zero initial crack length and neglecting the friction effect at the interface, the critical load for a fully propagated interfacial crack along the nanotube–polymer interface, F_c, is given by[21]

$$F_c = \pi \cdot D_{nt} \cdot \sqrt{\frac{E_{nt} \cdot G_c \cdot D_{nt}}{2\left(1 + \operatorname{csch}^2(2n \cdot l / D_{nt})\right)}}, \quad (1)$$

where E_{nt} is the nanotube's Young's modulus; G_c is the interfacial fracture energy; n is a parameter given by $n = \sqrt{\frac{E_m}{E_{nt}(1+\nu_m)\cdot\log(2R/D_{nt})}}$, in which E_m and ν_m are the Young's modulus and Poisson's ratio of the polymer matrix, respectively; R is the distance from the axis of the tube to the point in the polymer matrix where traction-free boundary conditions are satisfied and is approximated as one-half of the total thickness of the thin-film polymer t as illustrated in Figure 1b (i.e. R = 0.8 μm in our test). The catastrophic failure of the CNT–PMMA interface as revealed by our *in-situ* experiments indicates that F_c can be taken as the measured pull-out force P.[9] Therefore, the interfacial fracture energy of the CNT–PMMA interface can be quantified by using Equation (1). Because the diameters of the tubes employed in our experiments are very close to the resolution limit of the employed SEM and thus could not be measured precisely on the spot, we employ the statistical values of the nanotubes' diameters as measured by AFM in the analysis of the interfacial strength. In the following analysis and discussion, we focus on the results obtained based on the median nanotube diameter (3.1 nm), which is considered to be most representative of the measured nanotube–polymer interfaces. The data based on the lower and upper limits of the nanotube diameter (i.e. 2.0 nm and 4.2 nm) are also calculated and summarized in **Table 1**. Through fitting the experimental data along the lower and upper bounds of the measured pull-out forces using Equation (1) (see the solid and dotted curves in Figure 6a), the interfacial fracture energy is calculated to be within 0.135–0.215 J·m^{-2} based on the median nanotube diameter. Considering the lower and upper bounds of the nanotube diameter, the full range of the interfacial fracture energy is obtained as 0.054–0.8 J·m^{-2}. The following parameters are employed in the calculation: E_{nt} = 1.0 TPa,[22] E_m = 2.0 GPa, and ν_m = 0.32.[23] In the theoretically predicted curves, the pull-out load first increases with the embedded length and then reaches a constant or saturated value. The critical embedded length is quantified from the theoretical curve as the length value that corresponds to a pull-out load that is 1% below the saturated value. The critical embedded length is measured to be within the range of 170 nm (D_{nt} = 2 nm) to 356 nm (D_{nt} = 4.2 nm), compared with the experimental data (310 nm). Our value of G_c is consistent with recently reported data on the interfaces of epoxy with CNTs (0.05–0.25 J·m^{-2})[9] and high-temperature treated and surface graphitized carbon nanofibers (0.65 ± 0.14 J·m^{-2}),[6] but lower than the value (0.9–36.9 J·m^{-2}) reported in ref. [12]. It is noted that our measured interfacial strength is ascribed to the non-bonded van der Waal interactions between nanotubes and polymers. Therefore, it is still meaningful to compare our data on CNT–PMMA interfaces with those reported on other types of CNT-polymer interfaces of a similar binding mechanism (e.g. CNT-epoxy interfaces).

Table 1. The predicted critical embedded tube length and the calculated interfacial fracture energy and shear strength of the CNT–PMMA interface based on our in-situ single-tube pull-out measurements.

Nanotube outer diameter [nm]	Predicted critical embedded tube length [nm]	Interfacial fracture energy [J·m^{-2}]	Interfacial shear strength [MPa]	
			τ_{max}	τ_{ave}
2.0	170	0.50–0.80	372 ± 65	68 ± 16
3.1	263	0.135–0.215	155 ± 27	44 ± 10
4.2	356	0.054–0.087	85 ± 14	32 ± 8

Next we examine the interfacial shear strength of the CNT–PMMA interface. It is well-known that the shear stress on the nanotube–polymer interface is distributed non-uniformly. The shear stress possesses its maximum value at the tube entry position and decays with the depth of the tube into the polymer. The maximum shear stress developed at the

nanotube–polymer interface when the pull-out event occurs, τ_{max}, is calculated using a model developed by Greszczuk,[24]

$$\tau_{max} = \frac{2P \cdot n}{\pi \cdot D_{nt}^2 \cdot \tanh(2n \cdot l / D_{nt})}. \quad (2)$$

Figure 6b shows the calculated maximum shear strength on the CNT–PMMA interface based on the median tube diameter. The majority of the data points fall into the range of 140–185 MPa, except for those two points with the lowest embedded lengths. Besides a relatively larger uncertainty in measuring short embedded length, Equation (2) suggests that the diameters of those two tested tubes may be lower than the median value. For instance, for the tube with an embedded length of 0.21 μm, the maximum shear strength would increase to 156 MPa if a tube diameter of 2.0 nm was used in the calculation. It is envisioned that the observed data scattering in the calculated maximum shear strength can be mitigated using the following two approaches: (1) choosing nanotubes of relatively large diameters (e.g. 20–30 nm) in the pull-out test such that their outer diameters can be quantitatively measured using a SEM electron beam; (2) performing the pull-out test inside a high resolution TEM. By considering all the data points in Figure 6b, the maximum shear strength for the CNT–PMMA interface and its root mean square (rms) value are calculated to be 155 ± 27 MPa. Our results are close to the data reported on the interface between graphitized carbon fiber and epoxy (133 ± 19 MPa).[6]

In addition, we calculate the commonly used average interfacial shear strength τ_{ave} by assuming a uniform shear stress along the entire nanotube–polymer interface (i.e. $\tau_{ave} = P/(\pi \cdot l \cdot D_{nt})$). The results are shown in Figure 6c, which displays an expected decreasing trend for the embedded length exceeding the critical value. For those tubes with short embedded lengths (<310 nm), the average interfacial shear strength is calculated to be within 32–68 MPa (see Table 1). Our results are consistent with the theoretically predicted values of 27.4–35.9 MPa for the interface formed by single-walled CNTs with PMMA based on molecular dynamics (MD) simulations,[25] and the experimental data reported on the CNT-epoxy interface (30 ± 7 MPa).[11] Figure 6c shows that significantly lower average interfacial shear strengths are obtained for those tubes whose embedded lengths are well above the critical value. Our results clearly indicate that it is important to take into account the critical embedded length in assessing the failure of the nanotube–polymer interface based on the value of the average interfacial shear strength. The interfacial strength may be greatly underestimated if the embedded length is far above the critical value.

3. Conclusion

In this paper, we present a study of the CNT–PMMA interfacial strength by using an in-situ nanomechanical single-tube pull-out test technique. With the aid of high resolution electron beam, our nanomechanical testing scheme, which is based on three-layer polymer/nanotube/polymer sandwich-like structures, can be used as a general technique for quantitative measurements of nanotube–polymer interfacial strength. Our measurements of the pull-out force for tubes with different embedded lengths clearly reveal the shear lag effect, which indicates that the effective shear load transfer on the nanotube–polymer interface is confined within the critical embedded length. Our analysis highlights that it is essential to take into account the critical embedded length in the evaluation of the nanotube–polymer interfacial strength based on the average interfacial shear strength. Our work is useful to better understand the local stress transfer on the nanotube–polymer interface.

4. Experimental Section

Double-walled carbon nanotubes (DWCNTs), purchased from Sigma-Aldrich Co., were synthesized by chemical vapor deposition methods. The nanotubes, originally in the form of dry powders, were first separated in deionized water using ultrasonication for two hours with the aid of ionic surfactants sodium dodecylbenzenesulfonate (NaDDBS). AFM characterization of the dispersed tubes was performed inside an XE-70 AFM from Park Systems operating in tapping mode at room temperature. Transmission electron microscopy (TEM) and Fourier transform infrared (FTIR) characterization of the dispersed tubes were performed using a JEM 2100F TEM (JEOL Ltd.) operated at accelerating voltages of 120–200 kV and a Nicolet 8700 FTIR Spectrometer from Thermo Electron Corp., respectively.

PMMA (50 000 in molecular weight, Sigma-Aldrich) was dissolved in toluene to form a 10 wt% solution. The CNT–PMMA sandwich structure was formed by first spin-coating a PMMA/toluene solution at a speed of 4000 rpm to form a thin PMMA layer on a fresh silicon substrate, followed by the depositions of a well-dispersed nanotube solution and then another PMMA layer. The thin-film sandwich composite was dried for three hours at 130 °C and its total film thickness after drying was measured to be 1.6 μm by AFM.

In situ single-tube pull-out measurements were performed inside a FEI Nanolab 600 dual-beam electron microscope. AFM force sensors employed in the pull-out tests are silicon AFM probes (model CSG 01, NT-MDT) with nominal spring constants of 0.01–0.08 $N \cdot m^{-1}$. The actual spring constant of each employed AFM cantilever was calibrated to be within 0.04–0.09 $N \cdot m^{-1}$ using a thermal tuning method based on equipartition theory.[26] For the pull-out test, an AFM force sensor was mounted to a 3D piezo manipulator stage (Klocke Nanotechnik, Germany)[19,27–29] that possesses 1 nm displacement resolution in the motion of X-Y-Z axes and was controlled to move at a rate of approximately 1 $\mu m \cdot s^{-1}$. The pull-out force is calculated as the product of the spring constant of the AFM force sensor and its deflection measured by the electron beam. The displacement measurement resolution using the electron beam is determined by the pixel resolution in the recorded SEM images and is measured to be 2–5 nm depending on the imaging magnification. The corresponding force resolution is calculated to be 0.5 nN or better.

Supporting Information

Supporting Information is available from the Wiley Online Library or from the author.

Acknowledgements

This work was funded by US Air Force Office of Scientific Research and American Chemistry Society-Petroleum Research Fund. We thank Dr. In-Tae Bae for his assistance with the TEM characterization. The FTIR, the HRTEM, and the single-tube pull-out measurements were performed using the facilities in the Analytical and Diagnostics Laboratory at Binghamton University's Small Scale Systems Integration and Packaging Center (S3IP).

[1] J. Baur, E. Silverman, *MRS Bulletin* **2011**, *32*, 328–334.
[2] O. Breuer, U. Sundararaj, *Polym. Composites* **2004**, *25*, 630–645.
[3] J. N. Coleman, U. Khan, W. J. Blau, Y. K. Gun'ko, *Carbon* **2006**, *44*, 1624–1652.
[4] M. Rahmat, P. Hubert, *Composites Sci. Technol.* **2011**, *72*, 72–84.
[5] A. H. Barber, S. R. Cohen, S. Kenig, H. D. Wagner, *Composites Sci. Technol.* **2004**, *64*, 2283–2289.
[6] T. Ozkan, Q. Chen, I. Chasiotis, *Composites Sci. Technol.* **2012**, *72*, 965–975.
[7] M. P. Manoharan, A. Sharma, A. V. Desai, M. A. Haque, C. E. Bakis, K. W. Wang, *Nanotechnology* **2009**, *20*, 295701.
[8] T. Tsuda, T. Ogasawara, F. Deng, N. Takeda, *Composites Sci. Technol.* **2011**, *71*, 1295–1300.
[9] Y. Ganesan, C. Peng, Y. Lu, P. E. Loya, P. Moloney, E. Barrera, B. I. Yakobson, J. M. Tour, R. Ballarini, J. Lou, *ACS Appl. Mater. Interfaces* **2011**, *3*, 129–134.
[10] A. H. Barber, S. R. Cohen, H. D. Wagner, *Appl. Phys. Lett.* **2003**, *82*, 4140.
[11] A. H. Barber, S. R. Cohen, A. Eitan, L. S. Schadler, H. D. Wagner, *Adv. Mater.* **2006**, *18*, 83–87.
[12] C. A. Cooper, S. R. Cohen, A. H. Barber, H. D. Wagner, *Appl. Phys. Lett.* **2002**, *81*, 3873–3875.
[13] C. A. Cooper, D. Ravich, D. Lips, J. Mayer, H. D. Wagner, *Composites Sci. Technol.* **2002**, *62*, 1105–1112.
[14] A. A. Mamedov, N. A. Kotov, M. Prato, D. M. Guldi, J. P. Wicksted, A. Hirsch, *Nat. Mater.* **2002**, *1*, 190–194.
[15] F. H. Gojny, M. H. G. Wichmann, B. Fiedler, K. Schulte, *Composites Sci. Technol.* **2005**, *65*, 2300–2313.
[16] F. H. Gojny, M. H. G. Wichmann, U. Köpke, B. Fiedler, K. Schulte, *Composites Sci. Technol.* **2004**, *64*, 2363–2371.
[17] J.-L. Bantignies, J.-L. Sauvajol, A. Rahmani, E. Flahaut, *Phys. Rev. B* **2006**, *74*, 195425.
[18] L. Liu, Y. Qin, Z.-X. Guo, D. Zhu, *Carbon* **2003**, *41*, 331–335.
[19] C. H. Ke, N. Pugno, B. Peng, H. D. Espinosa, *J. Mech. Phys. Solids* **2005**, *53*, 1314–1333.
[20] M. Duchamp, R. Meunier, R. Smajda, M. Mionic, A. Magrez, J. W. Seo, L. Forró, B. Song, D. Tománek, *J. Appl. Phys.* **2010**, *108*, 084314.
[21] K. R. Jiang, L. S. Penn, *Composites Sci. Technol.* **1992**, *45*, 89–103.
[22] E. W. Wong, P. E. Sheehan, C. M. Lieber, *Science* **1997**, *277*, 1971–1975.
[23] J. Zeng, B. Saltysiak, W. S. Johnson, D. A. Schiraldi, S. Kumar, *Composites B: Engin.* **2004**, *35*, 173–178.
[24] P. S. Chua, M. R. Piggott, *Composites Sci. Technol.* **1985**, *22*, 33–42.
[25] Q. Zheng, Q. Xue, K. Yan, X. Gao, Q. Li, L. Hao, *J. Appl. Phys.* **2008**, *103*, 044302.
[26] E. L. Florin, M. Rief, H. Lehmann, M. Ludwig, C. Dornmair, V. T. Moy, H. E. Gaub, *Biosens. Bioelectron.* **1995**, *10*, 895–901.
[27] C. H. Ke, H. D. Espinosa, *Small* **2006**, *2*, 1484–1489.
[28] M. Zheng, C. H. Ke, *Small* **2010**, *6*, 1647–1655.
[29] C. H. Ke, M. Zheng, G. W. Zhou, W. L. Cui, N. Pugno, R. N. Miles, *Small* **2010**, *6*, 438–445.

Received: November 7, 2012
Published online: April 18, 2013